Placenta xxx (xxxx) xxx

Contents lists available at ScienceDirect

Placenta

journal homepage: www.elsevier.com/locate/placenta

Correlative three-dimensional X-ray histology (3D-XRH) as a tool for quantifying mammalian placental structure

Davis Laundon [a,b,*], Thomas Lane [c], Orestis L. Katsamenis [b,d], Jeanette Norman [e], Lois Brewer [f], Shelley E. Harris [a], Philip J. Basford [b,d,f], Justine Shotton [g], Danielle Free [g], Georgina Constable-Dakeyne [g], Neil J. Gostling [b,c], Pascale Chavatte-Palmer [h,i], Rohan M. Lewis [a,b]

[a] The Institute of Developmental Sciences, Human Development and Health, Faculty of Medicine, University of Southampton, Southampton, SO16 6YD, UK
[b] Institute for Life Sciences, University of Southampton, University Rd, Highfield, Southampton, SO17 1BJ, UK
[c] School of Biological Sciences, Faculty of Environmental and Life Sciences, University of Southampton, University Rd, Highfield, Southampton, SO17 1BJ, UK
[d] μ-VIS X-Ray Imaging Centre, Faculty of Engineering and Physical Sciences, University of Southampton, Southampton, SO17 1BJ, UK
[e] Histochemistry Research Facility, Faculty of Medicine, University of Southampton, Southampton, SO16 6YD, UK
[f] School of Engineering, Faculty of Engineering and Physical Sciences, University of Southampton, University Road, Southampton, SO17 1BJ, UK
[g] Marwell Wildlife, Thompson's Ln, Colden Common, Winchester, SO21 1JH, UK
[h] Université Paris-Saclay, UVSQ, INRAE, BREED, 78350, Jouy-en-Josas, France
[i] Ecole Nationale Vétérinaire d'Alfort, BREED, 94700, Maisons-Alfort, France

ARTICLE INFO

Keywords:
Placenta
microCT
Histology
Comparative
Structure

ABSTRACT

Mammalian placentas exhibit unparalleled structural diversity, despite sharing a common ancestor and principal functions. The bulk of structural studies in placental research has used two-dimensional (2D) histology sectioning, allowing significant advances in our understanding of mammalian placental structure. However, 2D histology sectioning may be limited if it does not provide accurate information of three-dimensional (3D) tissue architecture. Here, we propose correlative 3D X-ray histology (3D-XRH) as a tool with great potential for resolving mammalian placental structures. 3D-XRH involves scanning a formaldehyde-fixed, paraffin embedded (FFPE) tissue block with 3D X-ray microscopy (microCT) prior to histological sectioning to generate a 3D image volume of the embedded tissue piece. The subsequent 2D histology sections can then be correlated back into the microCT image volume to couple histology staining (or immunolabelling) with 3D tissue architecture. 3D-XRH is non-destructive and requires no additional sample preparation than standard FFPE histology sectioning, however the image volume provides 3D morphometric data and can be used to guide microtomy. As such, 3D-XRH introduces additional information to standard histological workflows with minimal effort or disruption. Using primary examples from porcine, bovine, equine, and canine placental samples, we demonstrate the application of 3D-XRH to quantifying placental structure as well as discussing the limitations and future directions of the methodology. The wealth of information derived from 2D histological sectioning in the biomedical, veterinary, and comparative reproductive sciences provides a rich foundation from which 3D-XRH can build on to advance the study of placental structure and function.

1. Introduction

Despite evolving only once and having conserved physiological functions, the mammalian placenta exhibits unparalleled structural diversity among organs [1–6]. The selective pressures governing the evolution of morphological divergence, and the functional consequences of structural diversity, are poorly understood. The bulk of our knowledge of mammalian placental structure is derived from two-dimensional (2D) histology sections [6]. Studies employing 2D histology sectioning have provided valuable insight into mammalian placental structure and laid the foundation for structural investigations into the placenta. However, 2D imaging techniques may have limitations for

* Corresponding author. Faculty of Medicine, MP 887, IDS Building, University of Southampton, Southampton General Hospital, Southampton, SO16 6YD, UK.
E-mail address: D.J.Laundon@soton.ac.uk (D. Laundon).

https://doi.org/10.1016/j.placenta.2024.07.312
Received 5 February 2024; Received in revised form 15 July 2024; Accepted 30 July 2024
Available online 31 July 2024

understanding placental structure if they do not accurately reflect the native three-dimensional (3D) architecture of the biological structures [6]. Indeed, extrapolating 3D placental structure from 2D images has been shown to be problematic [7]. 3D imaging of the placenta is also important for anatomy, pathology, and as a basis for mathematical modelling of placental function [8–10].

3D imaging therefore presents an opportunity to better quantify mammalian placental structures in their native 3D. However, choosing any single imaging technique comes with inherent trade-offs. The most obvious is the trade-off between spatial resolution and volume of tissue imaged, with higher resolution datasets typically limited to a smaller biovolumes [11]. Other trade-offs can be just as influential in choosing an imaging technique, such as the restriction of imaging modalities from differences in sample preparation. For example, the strong chemical fixation and heavy-metal staining steps needed for standard high-resolution electron microscopy imaging typically quench fluorescence [12] and remove fluorescence microscopy as an option for these samples. Correlative imaging workflows are therefore designed to overcome such limitations by applying multiple imaging modalities to the same sample to exploit their benefits while mitigating against their trade-offs [13].

Correlative 3D X-ray histology (3D-XRH) (Fig. 1, Table 1) is a novel technique whereby formalin-fixed, paraffin-embedded (FFPE) tissue samples are non-destructively scanned by 3D X-ray microfocus computed tomography (microCT) prior to histology sectioning and staining [14]. This produces a 3D image volume of the embedded tissue sample with minimal effort which is then automatically 'virtually sliced' into a serial image stack that can be used to both select a location of interest for histology sectioning and to quantify the 3D architecture of specific biological structures within the sample. The resulting stained histology section(s) can then be correlated back into the microCT volume to identify structures from differential staining or examine individual slices at higher resolution. Correlative 3D-XRH workflows have been applied to diverse tissue types, including lung [14,15], pancreas [16], and whole horse embryos [17]. 3D-XRH is therefore a powerful tool for coupling multidimensional imaging modalities and quantifying microscale tissue architecture, particularly in biomedical research fields

Table 1
– Comparative aspects of 2D histology sectioning and 3D microCT imaging. Correlative 3D-XRH gives the benefits of both modalities.

Parameter	Histology sectioning	microCT imaging
2D information	✓	✓
Isotropic 3D information	×	✓
Non-destructive	×	✓
Staining	✓	×
Pixel/voxel size	<1 μm	>1 μm (typically3–10 μm)
Image output type	RGB	Greyscale
Immunolabelling	✓	×
Multiscale	×	✓

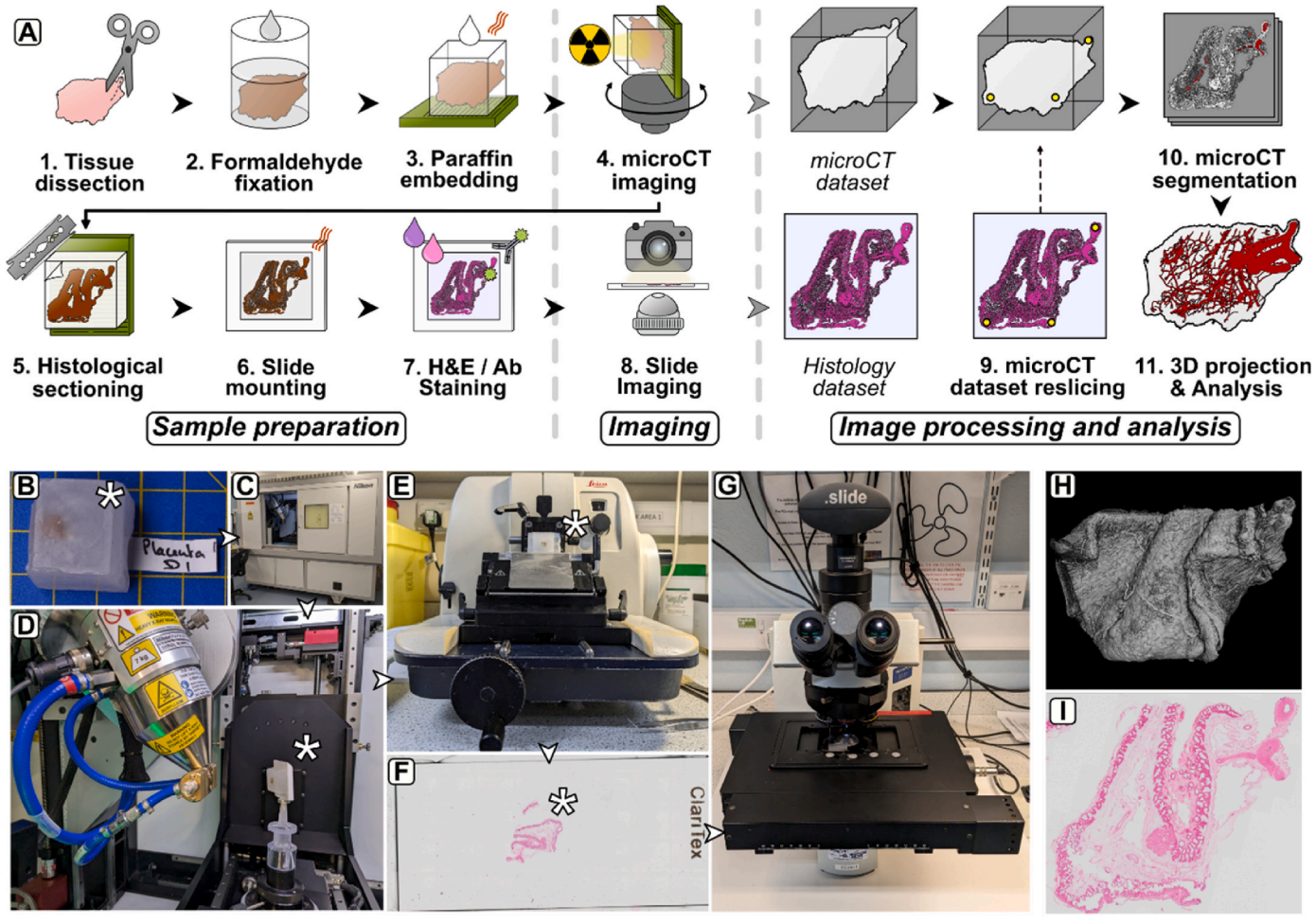

Figs. 1. 3D X-ray histology (XRH) is a powerful tool for resolving placental structure. (A) Diagrammatic summary of the workflow used in this paper. This workflow is adapted from that detailed in Ref. [14]. (B–G) Illustrative steps in our 3D-XRH workflow. Formalin-fixed, paraffin-embedded (FFPE) blocks (B) are imaged in a microCT scanner (C&D) prior to microtomy (E). Tissue sections are then stained with H&E (or immunolabelled) (F) and imaged on a slide scanner (G). The outputs of this workflow are both a 3D volume X-ray dataset (H) and 2D stained histology sections (I) of the same tissue sample. Asterisk marks the sample.

where a large historic focus on 2D histology sectioning can be used to 'ground-truth' 3D structures derived from microCT.

We propose that 3D-XRH would be a powerful tool to introduce to the study of placental structure. Given the large amount of 2D histology data previously used in describing mammalian placental structures, 3D-XRH presents the logical next step in expanding this understanding in 3D. Here, we discuss the benefits of 3D-XRH and outline the central workflow. We demonstrate its applicability in comparative placentation by showing worked examples using FFPE placental samples from pig, cow, horse and zebra, and dog.

2. Method and Materials

Below, we detail the protocol we have used to generate the 3D-XRH datasets of mammalian placental samples shown in this work (Fig. 1). Parameters and equipment can be altered to accommodate different samples and research environments; however, the central principles will remain the same. This protocol is adapted from that detailed in Ref. [14]. We do not intend to claim that this protocol would not benefit from further optimisation, such as experimental refinement of fixation/embedding protocols to prevent tissue shrinkage, however to help users more easily add 3D-XRH to their current histology workflows we have written the protocol in line with standard FFPE histology protocols. This also has the benefit of allowing users to apply 3D-XRH to historic FFPE tissue samples previously embedded for standard histology.

2.1. Sample collection and ethics

Pig, cow, horse, and dog placentas were collected as part of ongoing veterinary studies. Pig (gestational day 100 (G100)) and cow (G90, G170, and G280) placentas were stored as supplementary samples in INRAE experimental farms during experimental protocols aiming at other purposes and previously validated by ethical committees. Horse placenta (term) was obtained by natural delivery at the experimental farm of Institut Français du Cheval et de l'Equitation (IFCE). The dog (G27) placenta was obtained at Alfort's veterinary school (ENVA) in France during spaying of pregnant bitches for clinical purposes. A zebra (term) placenta was collected after delivery at Marwell Wildlife, UK. Sample analysis in Southampton received local approval from the University of Southampton (47770.A1/46381.A2).

2.2. Tissue dissection, fixation, and embedding

Placental tissue should be dissected and fixed as soon as possible following collection to best preserve microscale structures.

1. To prevent desiccation during dissection, the tissue was submerged in buffer 1 x phosphate buffered saline pH 7.4.
2. Under a stereo microscope, <1 cm^3 tissue samples of interest were excised with fine dissecting scissors.
3. The dissected tissue was fixed in buffered fixative (4 % formaldehyde in 1 x phosphate buffered saline pH 7.4) overnight at room temperature and stored at 4 °C prior to embedding.
4. Fixed tissue pieces were embedded into paraffin wax blocks using a HistoStar embedding workstation. (ThermoFisher Scientific). To optimise downstream histological sectioning, orient the sample so that the desired XY block face runs perpendicular to the cutting axis.

Note: It helps to place the tissue between sponges in the cassettes during processing to ensure that the sample remains flat.

2.3. microCT-based 3D X-ray histology imaging

All microCT imaging was conducted at the μ-VIS X-ray Imaging Centre (www.muvis.org), 3D X-ray Histology Facility at the University of Southampton.

5. FFPE tissue blocks were imaged using a custom Nikon XTH 225 ST microCT scanner (Nikon X-Tek systems Ltd) operating at peak voltage of 80 kV. Source-to-object and source to detector distances were 37.2 mm and 933.1 mm respectively generating datasets at 6.0 μm isotropic voxels. Acquisition was conducted by collecting 3001 projections over a 360° angular range (angular step: 0.12°).
6. Following the acquisition process, the radiographic data were reconstructed into 32-bit.vol files using the built-in reconstruction software which used a filtered back projection algorithm. This ensures that there are no over- or under-saturated voxels in the generated volume, and appropriate "windowing" can be selected further down the line according to the needs of the analysis.
7. Following reconstruction, the 32-bit raw volumes were brought into Fiji/ImageJ software (NIH, Bethesda, MD; http://imagej.nih.gov/ij) [18].
8. The XRH datasets were roughly aligned (resliced) to simulate the traditional histological slicing of a tissue block when navigating through the stack along the XY plane. This requires subsequent rotations and reslicing across the three orthogonal planes. The process is semi-automated using the "histological relevant reslice" script, available through the XRH processing toolbox [19]. The script requires the user to draw a line parallel to the wax/air interface, measures the angle of that line, and, using that information, rotates the volume so that the interface becomes parallel to the Y-axis of the image and orthogonal to X. It then reslices the volume across the XZ plane and repeats the process. This process ensures that each XY slice within the image stack is parallel to the histology cassette, if applicable, so that scrolling through XY slices progresses from the surface of the wax block towards the cassette, mirroring the motion of a microtome knife during the physical sectioning in conventional histology workflows (refer to Video 1 in Ref. [20]).
9. A 3D median filter ($2 \times 2 \times 2$ kernel) was then employed, followed by a 2D unsharp mask (Gaussian blur factor $= 3$ pixels), applied to each reconstructed slice of the microCT stack using a custom script (available through the XRH toolbox; https://doi.org/10.5281/zenodo.8252047). This approach improves the signal-to-noise and contrast-to-noise ratios, serving both visualisation and segmentation workflows.
10. Upon completion, the grey levels were linearly windowed to a range of $(-50, 100)$, encompassing X-ray attenuation information related to soft tissue, paraffin wax, and the surrounding air. Images were then converted to 16-bit and saved as .raw volume files.

2.4. Histology sectioning, staining, and slide scanning

This step is destructive to the sample, so make sure all microCT imaging is finished and the datasets satisfactory prior to proceeding. A single slice through the sample is sufficient to realign and correlate the microCT dataset, however take as many slices as desired to identify structures of interest through the tissue volume.

11. FFPE tissue blocks were cut using an RM2135 Manual Rotary Microtome (Leica) to generate 4 μm thin sections. Blocks were kept on ice if not mounted in the microtome to keep the wax cold as warmer sections are more likely to tear.
12. Sections were kept flat using a paintbrush and gently transferred to a 45 °C water bath for $\geq$30 s.
13. Sections were placed on slides by submerging the slides underneath the floating sections. Sections were adhered to the slides by melting the wax in an incubator at 37 °C for $\geq$48 h.

Note: Sections destined just for haematoxylin and eosin (H&E)

staining can be dried on a hot plate at 60 °C for 0.5–1 h after sectioning, however this is inappropriate for immunohistochemistry applications as this temperature can denature target proteins.

14. Histology slides were stained with H&E using a standardised protocol to visualise cellular and tissue structures. Any H&E protocol optimised for specific FFPE tissue samples or applications can be used.
15. Stained slides were imaged using a dotSlide Virtual Microscopy System slide scanner (Olympus) under a 40x objective lens generating large images with an XY pixel resolution of 0.35 μm.

2.5. Image registration, segmentation, and quantification

Image datasets were correlated, segmented, and quantified as detailed step-by-step in Ref. [11]. Image processing will require manual oversight, and can therefore be labour-intensive for large datasets, but following the semi-automatic steps below can rapidly decrease image processing time.

16. Processed microCT datasets were further resliced to precisely correlate the z-depth to the histological block face cutting axis. For this, three distinct tissue landmarks were identified in the histological section. microCT datasets were loaded into Avizo (ThermoFisher Scientific) and then the tissue landmarks from the histological section were located within the z-stack and their XYZ coordinates recorded. The three landmark XYZ coordinates were then used to reslice the microCT dataset to the new orientation. As stated above, the microCT dataset will be processed to be approximately at the orientation of the physical block face, so these adjustments should be minimal in practice.
17. The resliced dataset can now be segmented in 3D. For these examples, datasets were loaded into Microscopy Image Browser (MIB) [21] and semi-manually segmented by masked intensity thresholding, followed by statistical thresholding and manual curation.
18. Segmented tissue structures were then quantified for metrics such as volume and surface area within MIB. For visualisation in

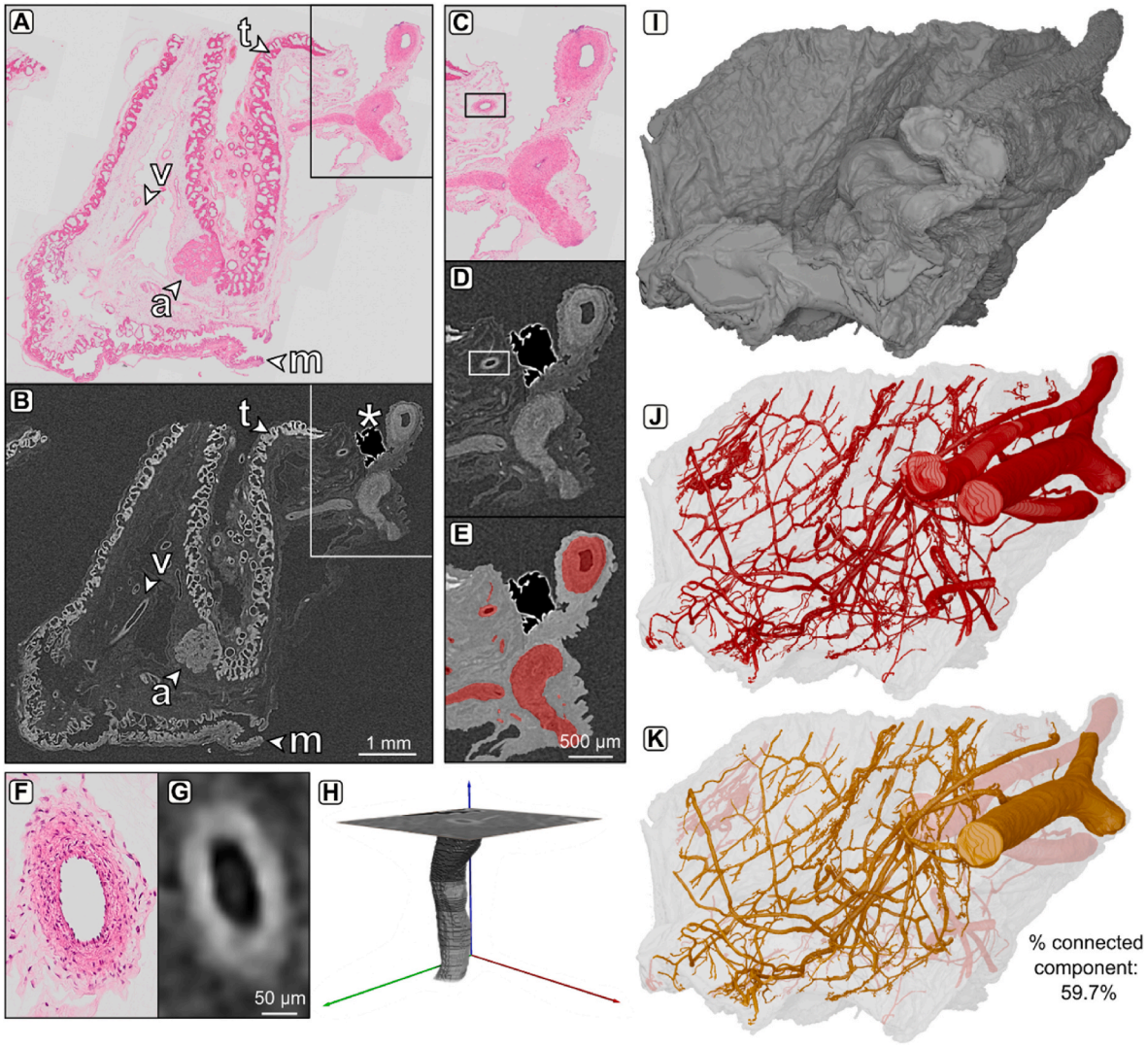

Fig. 2. Worked example of the output from this correlative 3D-XRH workflow in a piece of porcine (pig) placenta. (A&B) 2D H&E histology image (A) and the corresponding slice through the 3D microCT dataset (B) of a piece of G100 pig placenta. Labelled are an areola (a), maternal tissue (m), trophoblast (t), and blood vessel (v). Asterisk points to a small air bubble in the paraffin wax outside of the tissue. (C–E) Inset of major blood vessels marked in (A&B) shown in the 2D histology image (C), microCT dataset (D), and segmented in the microCT dataset (E). Blood vessels (red) and other tissue (grey). (F–H) Inset of a single blood vessel highlighted in (C&D) shown in the 2D histology image (F), 2D microCT slice (G), and volume render from a cropped 128 voxel cube from the 3D microCT dataset (H). (I–K) 3D reconstruction of the tissue piece from the 3D microCT dataset showing tissue exterior (I), blood vessels (red) (J), and the largest connected component from the blood vessel reconstruction (orange) (K). An image using this piece of G100 pig placenta was previously published in Ref. [6].

figures, surface meshes of segmented structures were generated in Avizo and rendered in Blender v.3.1.2 (blender.org).

3. Example Results

Using the 3D-XRH workflow outlined above, we generated correlative 2D H&E histology-3D microCT image datasets for pieces of mammalian placental tissue. H&E staining is by far the most common method for visualising cellular and tissue structures in histology sections [22,23], making comparison easy with the wealth of previous literature in comparative placentation. Correlative H&E sections in this study could therefore be used to identify structures in the greyscale microCT datasets and 'ground-truth' them in the established literature.

In this example, H&E staining was used to identify an areola, maternal tissue, fetal trophoblast, and blood vessels in a piece of G100 (gestational day 100) porcine (pig) placental tissue (Fig. 2A&B) from previous literature e.g. Ref. [24]. To illustrate the benefit of 3D-XRH in comparative placentation, we identified and segmented the blood vessel network in this piece of tissue (Fig. 2C–E). Side-by-side comparison of a mid-sized blood vessel between 2D H&E histology (Fig. 2F) and microCT (Fig. 2G) highlights the trade-offs between the individual modalities. 2D histology presents a much higher XY resolution than microCT and can resolve individual endothelial cells, however it lacks the 3D connectivity of microCT (Fig. 2H). 3D reconstruction of the blood vessel network enables the visualisation of its complex hierarchical branching structure (Fig. 2I and J). From this, connectivity can be calculated, and the largest connected component extracted, visualised, and quantified (Fig. 2K).

In tightly interdigitated placental structures such as placentomes, labelling structures as fetal or maternal can be difficult. This is because 2D histology sections lack connectivity to resolve tissue context, yet microCT datasets lack staining information identifying organismal origin. We used 3D-XRH to identify and segment areas of fetal and maternal tissue across gestational time points in bovine (cow) placentomes (Fig. 3A–C). Previous literature has shown that maternal tissue stains more purple (haematoxylin-rich) than pinker (eosin-rich) fetal tissue [25]. This permitted us to 3D reconstruct and visualise the architecture of maternal septa at different time points, and quantify their volumetric contribution to the sample (Fig. 3D). Using a cropped cube from a microCT dataset of tightly interdigitated placentome tissue, we used 3D-XRH to assign the relative contributions of fetal and maternal tissue (Fig. 3E–H). Unfortunately, there is some fine tissue shrinkage on the fetal side of this sample that occurred during fixation, but the

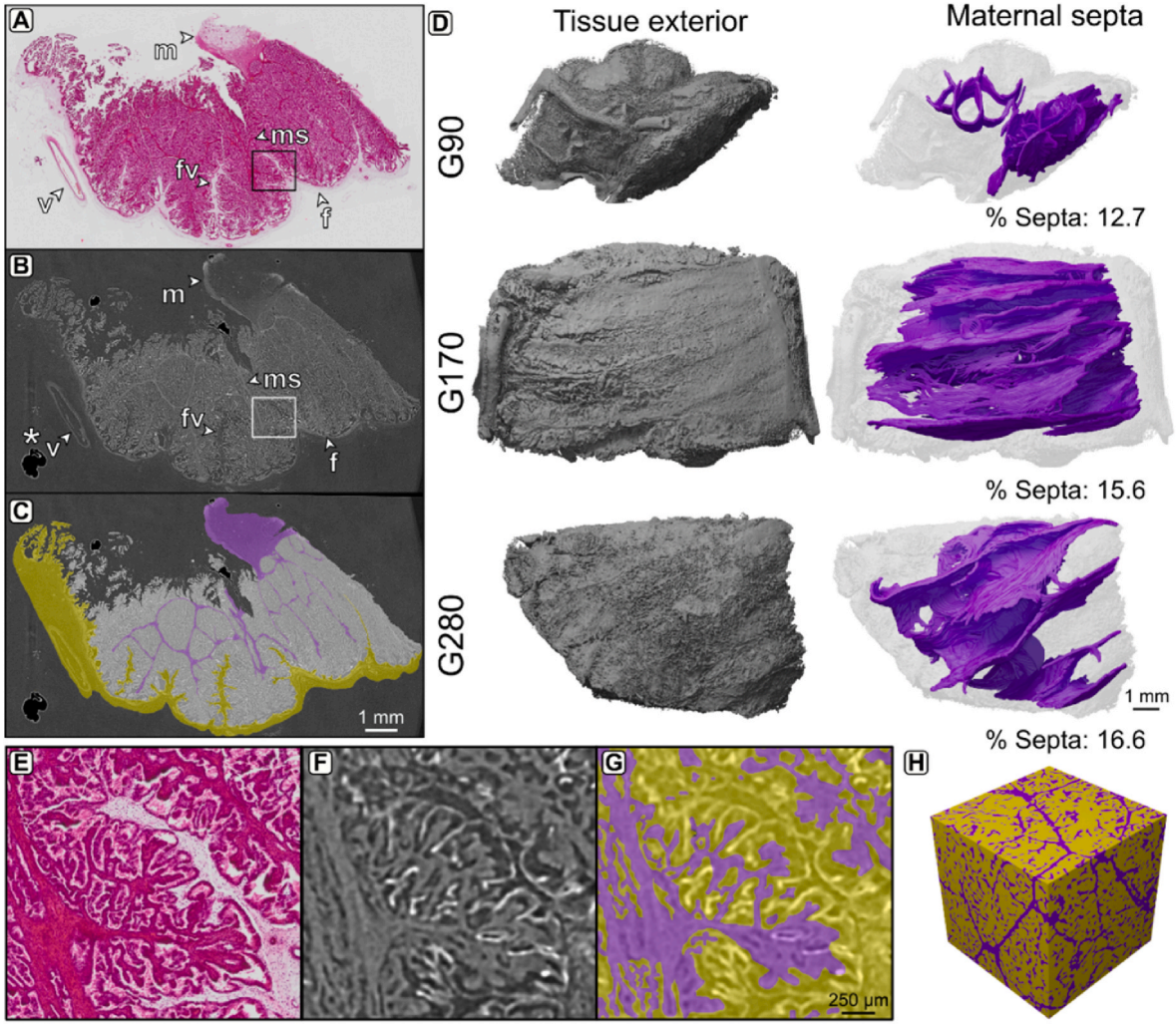

Fig. 3. – 3D-XRH reconstruction and quantification of fetal and maternal tissue in bovine (cow) placentomes across gestation. (A–C) 2D H&E histology image (A), corresponding slice through the 3D microCT dataset (B), and segmented microCT slice (C) of a piece of G90 cow placentome. Labelled are the fetal side of the placentome (f), major fetal villus (fv), maternal side of placentome (m), major maternal septa (ms), and a blood vessel (v). Segmented are the major parts of the fetal (yellow) and maternal (purple) contributions to the placentome, with tightly interdigitated tissue (grey). (D) 3D reconstruction of tissue pieces from the 3D microCT dataset showing tissue exterior (grey) and maternal septa (purple) for different time points. (E–G) Inset marked in (A&B) shown in the 2D histology image (E), microCT dataset (F), and segmented in the microCT dataset (G). (H) Segmentation shows major fetal (yellow) and maternal (purple) tissue contributions.

example still illustrates the potential of 3D-XRH for placentome biology. Further refinement of tissue fixation protocols, perhaps using different fixatives or embedding procedures, could mitigate against fine tissue shrinkage in the future iterations of this workflow.

3D connectivity is particularly important for villous placentas as there is evidence to suggest that extrapolating the 3D structure of branching placental villi is problematic from 2D data [7]. We used 3D-XRH to identify and segment the chorionic villous surface of equine (horse and zebra) placentas (Fig. 4A–E) [26,27]. 3D reconstruction permitted quantification of the villous surface area important for feto-maternal nutrient exchange in its native 3D (Fig. 4F and G). The connectivity of the 3D microCT dataset can be used to trace the origin of individual villi, such as those associated with microcotyledons (Fig. 4H) or those originating from the chorionic surface in between microcotyledons (Fig. 4I).

The canine placenta, and its maternal interface, consists of a of series of tissue layers that vary radically in structural composition [24,28]. Using 3D-XRH, we identified and reconstructed these layers in 3D (Fig. 5A–G). Almost all tissue layers could be clearly identified and segmented in the microCT dataset, however the chorionic plate was low opacity and was therefore reconstructed by manual tracing and interpolation. It is therefore displayed in Fig. 5 as approximate. Our segmentation enabled the quantification of these layers by their volumetric contribution to the tissue sample (Fig. 5H) and surface area to volume ratio (SA:V) (Fig. 5I). Ranking tissue layers by SA:V highlights those which contribute to secretion or uptake disproportionately to their volume (Fig. 5I). Of course, these values are the given SA:V at this scale of investigation and additional finer scales (inclusive of nanostructures such as microvilli or fine maternal vessels) would need to be incorporated for a holistic understanding of materno-fetal exchange surfaces. Immunofluorescent staining of this sample of canine placenta, targeting vimentin to label stromal cells and counterstained with DAPI to visualise nuclei, highlights the compatibility of 3D-XRH with immunolabelling and shows how molecular information can be correlated with 3D microstructure (Fig. 2J and K).

4. Discussion

Here, we have outlined the principles behind 3D-XRH and highlighted the benefits of applying this methodology to quantifying placental structure through worked examples. Since the bulk of what we know of mammalian placental structure is derived from 2D H&E histology stains [6], 3D-XRH presents an easy way to use these data to identity structures from X-ray microscopy and introduce 3D structural information to these datasets. We used 3D-XRH to reconstruct and quantify the blood vessel network of a piece of porcine placenta, the maternal septa from bovine placentomes at different gestational time points, the villous surface area of equine placentas, and the tissue layers in a piece of canine placenta as a demonstration of these principles.

The individual trade-offs of 2D H&E histology and 3D microCT can be mitigated against, and their benefits exploited, by coupling the two methods into a correlative 3D-XRH workflow. Our 3D-XRH datasets provided both high-resolution, differentially-stained 2D structural information and quantitative 3D architecture for every tissue sample, expanding the amount of information available for investigation. Although technically it is possible to serially section and image an entire paraffin tissue block, such imaging would be extremely laborious, time consuming, destructive, and prone to section loss. For reference, assuming a ~5 μm physical histology section thickness (comparable to our virtual z-pixel depth), a ~1 cm tissue cube would require ~2000 slices to be imaged in its entirety (comparable to the number of virtual slices in our 3D-XRH example datasets above), which would be a colossal amount of work for any given researcher to section manually. Adding microCT imaging prior to histological sectioning is advantageous as it requires no additional sample prep beyond that already necessitated for FFPE histology and is relatively effortless, quick, entirely non-destructive, and not subject to section loss. Having knowledge of the 3D arrangement of a given tissue piece can also guide

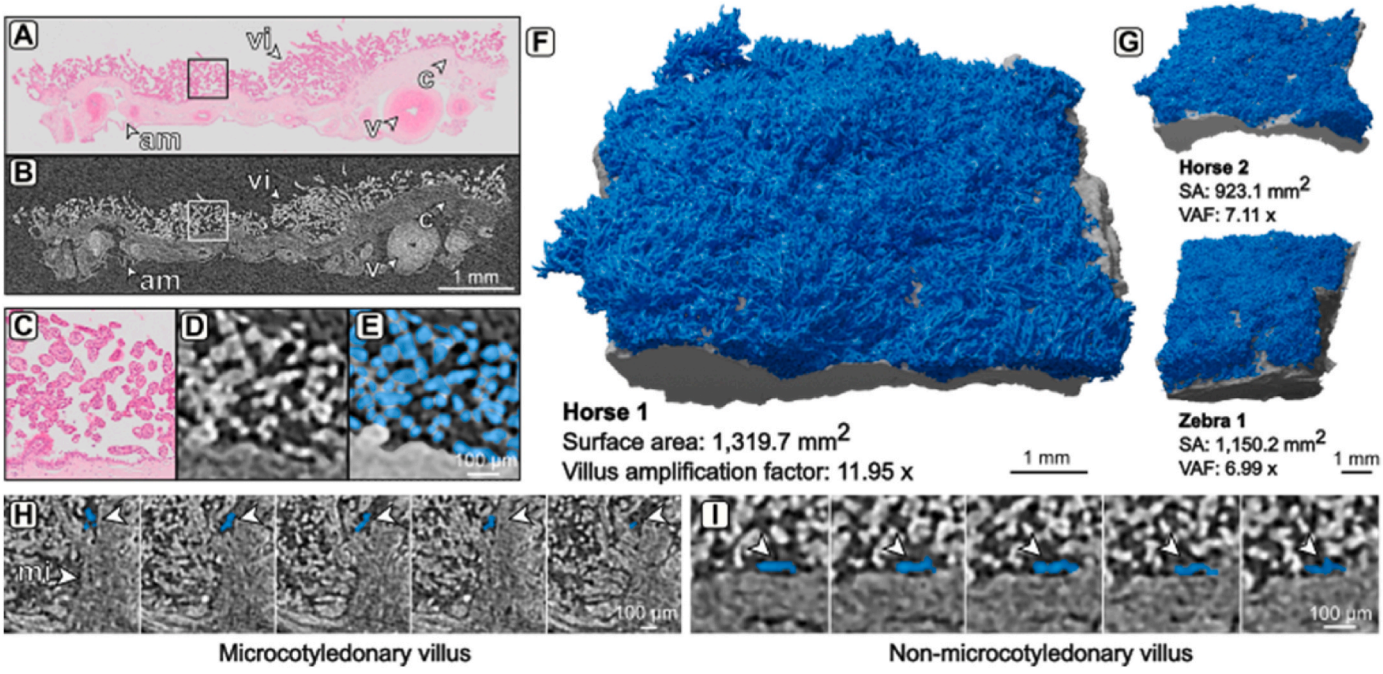

Fig. 4. – 3D-XRH reconstruction and quantification of equine (horse and zebra) placental villi. (A&B) 2D H&E histology image (A) and the corresponding slice through the 3D microCT dataset (B) of a piece of term horse placenta. Labelled are the allantoic membrane (am), chorion (c), blood vessel (v), and villi (vi). (C–E) Inset of placental villi marked in (A&B) shown in the 2D histology image (C), microCT dataset (D), and segmented in the microCT dataset (E). Villi (blue) and other tissue (grey). 3D reconstruction of samples from the 3D microCT dataset showing villi (blue) and other tissue (grey), in a piece of term horse placenta (F) and other pieces of horse and zebra placenta (G). (H–I) 3D-XRH datasets can be used to resolve the connectivity of individual villi. Shown are a villus that connects to a microcotyledon (mi) (H) and a villus that connects to the non-microcotyledonary tissue surface (I).

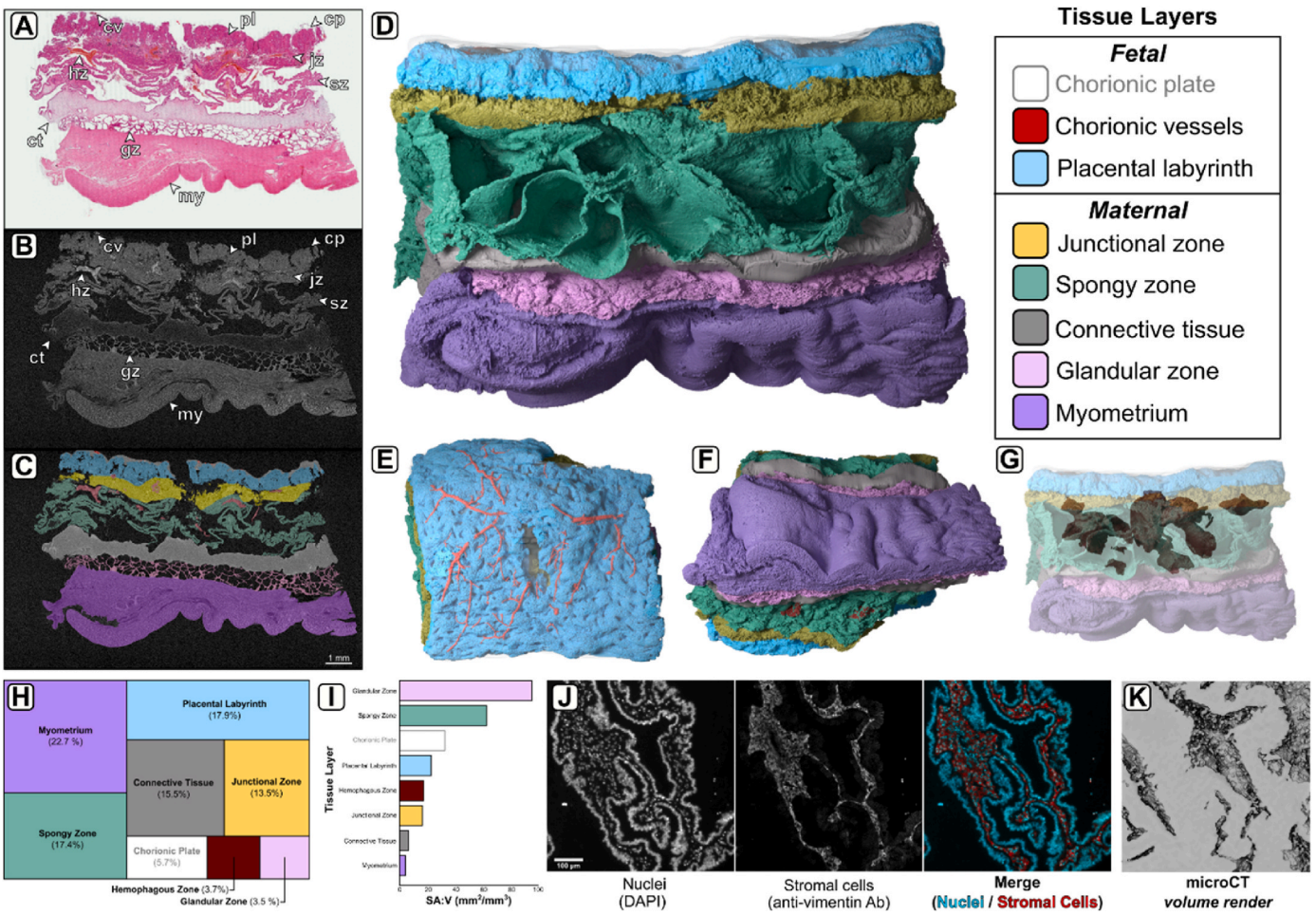

Fig. 5. – 3D-XRH reconstruction and quantification of tissue layers in a piece of canine (dog) placenta. (A&B) (A-C) 2D H&E histology image (A), corresponding slice through the 3D microCT dataset (B), and segmented microCT slice (C) of a piece of G27 dog placenta. Colours in (C) are as in the legend in (D). (D-G) 3D reconstruction of the microCT dog placenta dataset showing all tissue layers (D), fetal-facing side (E), maternal-facing side (F), and the hemophagous zones (G). (H-I) Quantification of the contributions of the tissue layers imaged by microCT by volume (H) and surface area to volume ratio (SA:V) (I). (J) Immunofluorescent staining of the spongy zone labelling nuclei (DAPI; cyan) and stromal cells of mesenchymal origin (anti-vimentin antibody (Ab); red) shown alongside the 3D structure from an (approximate) correlative subvolume from the microCT dataset (K).

microtomy by informing which z-depth into the block tissues of interest reside prior to sectioning. Taken together, 3D-XRH shows clear benefits when incorporated into histology studies in placental research.

As within any imaging modality, correlative 3D-XRH also has limitations. Previously, we have published a workflow for correlative microCT-vEM (3D volume electron microscopy) of placental tissue [11, 29] which employs heavy metal staining (as contrasting agents) and resin embedding prior to microCT imaging. The 3D-XRH workflow described here has advantages over our microCT-vEM workflow in that it permits the imaging of larger pieces of tissue ($<\sim$1 cm^3 versus $<\sim$3–5 mm^3) and, due to the lack of heavy tissue processing, leaves tissue pieces largely innate for downstream staining or immunolabelling. However, this same lack of tissue processing, and the similar X-ray attenuation levels of biological tissues and paraffin wax, means image datasets from 3D-XRH are of much lower contrast than in microCT-vEM, which can make segmentation challenging and more laborious. Also, 3D-XRH generates bigger block face 2D sections than in microCT-vEM. 3D-XRH wax sections are also softer than the resin sections taken in microCT-vEM. Taken together, these factors mean the 2D slices used to reslice 3D microCT datasets are more likely to be deformed in 3D-XRH. Practically speaking, this has little impact on the qualitative image correlation shown in this study, but for quantitative voxel-to-voxel registration, sophisticated image warping algorithms would be necessary [14].

Despite these limitations, 3D-XRH still offers great future scope for research in comparative placentation. As tissue is processed using standard FFPE protocols, immunolabelling with chromogenic or fluorogenic antibodies can be used to target proteins of interest in 2D histology sections and couple molecular profiling with 3D quantification of the associated tissue architecture (Fig. 2J and K). Artificial intelligence algorithms, be they based on 'deep' machine learning techniques or user supervised 'shallow' learning techniques, could be employed in the future to improve the segmentation of lower contrast images generated by 3D-XRH. For deep learning, software such as Deep MIB [30] that use manually segmented training datasets to train neural network classifiers to label tissue structures of interest could be used for 3D-XRH datasets. For shallow learning, software such as Weka [31] or Ilastik [32] can be used alongside user intervention and feedback to train classifiers. Future application of such approaches should further improve 3D-XRH workflows and widen its applicability to placental research beyond comparative placentation. With a proper randomised systematic approach to avoid bias in sampling, 3D-XRH could also be used within clinical applications, such as comparing the villus structure between control and pathological placentas, or by coupling changes in molecular expression identified from immunohistochemistry with changes to 3D tissue architecture.

5. Concluding Remarks

Most of our understanding of mammalian placental structure is derived from 2D histological sectioning. Although these data have contributed greatly to characterising placental structure, they are limited by not reflecting 3D tissue architecture. We therefore propose 3D-XRH as an opportunity to build on the rich resources of placental histology sectioning. Here, we show worked examples of 3D-XRH on non-human placental tissue to reconstruct and quantify placental structures. These examples demonstrate the applicability of 3D-XRH to resolve and quantify complex 3D tissue structures in the mammalian placenta.

Funding

This work was funded by Leverhulme Trust grant number RPG-2019-208. Equipment in the Biomedical Imaging Unit was supported by MR/L012626/1 Southampton Imaging under MRC UKRMP Funding.

Data Accessibility

All image datasets and corresponding labels associated with this publication are freely available for download at Bioimage Archive accession S-BIAD1270 under license CC BY 4.0 https://www.ebi.ac.uk/biostudies/bioimages/studies/S-BIAD1270.

CRediT authorship contribution statement

Davis Laundon: Writing – review & editing, Writing – original draft, Visualization, Validation, Resources, Project administration, Methodology, Investigation, Formal analysis, Data curation, Conceptualization. **Thomas Lane:** Writing – review & editing, Investigation, Formal analysis, Data curation. **Orestis L. Katsamenis:** Writing – review & editing, Writing – original draft, Methodology, Investigation, Formal analysis, Data curation. **Jeanette Norman:** Writing – review & editing, Writing – original draft, Methodology, Investigation, Formal analysis, Data curation. **Lois Brewer:** Writing – review & editing, Investigation, Formal analysis, Data curation, Conceptualization. **Shelley E. Harris:** Writing – review & editing, Investigation, Formal analysis, Data curation. **Philip J. Basford:** Writing – review & editing, Investigation, Formal analysis, Data curation. **Justine Shotton:** Writing – review & editing, Resources. **Danielle Free:** Writing – review & editing, Resources. **Georgina Constable-Dakeyne:** Writing – review & editing, Resources. **Neil J. Gostling:** Writing – review & editing, Supervision, Resources, Project administration, Funding acquisition. **Pascale Chavatte-Palmer:** Writing – review & editing, Writing – original draft, Supervision, Project administration, Investigation, Funding acquisition. **Rohan M. Lewis:** Writing – review & editing, Writing – original draft, Supervision, Resources, Project administration, Funding acquisition, Formal analysis, Data curation, Conceptualization.

Declaration of competing interest

We declare we have no competing interests.

Acknowledgements

We acknowledge the μ-VIS X-ray Imaging Centre, part of the National Facility for laboratory-based X-ray CT (nxct.ac.uk – EPSRC: EP/T02593X/1), the Biomedical Imaging Unit at the University of Southampton for the provision of imaging, processing, and data management infrastructure, and the Histochemistry Research Facility at the University of Southampton for providing access to histology equipment.

References

[1] R. Leiser, P. Kaufmann, Placental structure - in a comparative aspect, Exp. Clin. Endocrinol. 102 (3) (1994) 122–134.
[2] F.B.P. Wooding, A.P.F. Flint, Placentation, Marshall's Physiology of Reproduction, 1994, pp. 233–460.
[3] D.E. Wildman, C.Y. Chen, O. Erez, L.I. Grossman, M. Goodman, R. Romero, Evolution of the mammalian placenta revealed by phylogenetic analysis, P Natl Acad Sci USA 103 (9) (2006) 3203–3208.
[4] O.W. Griffith, G.P. Wagner, The placenta as a model for understanding the origin and evolution of vertebrate organs, Nat Ecol Evol 1 (4) (2017) 72.
[5] G.J. Burton, Placental Types, Benirschke's Pathology of the Human Placenta, Springer Nature, Switzerland, 2022, pp. 23–38.
[6] D. Laundon, N.J. Gostling, B.G. Sengers, P. Chavatte-Palmer, R.M. Lewis, Placental evolution from a three-dimensional and multiscale structural perspective, Evolution 78 (2023) 13–25.
[7] E. Haeussner, B. Aschauer, G.J. Burton, B. Huppertz, F.E. von Koch, J. Muller-Starck, C. Salafia, C. Schmitz, H.G. Frank, Does 2D-Histologic identification of villous types of human placentas at birth enable sensitive and reliable interpretation of 3D structure? Placenta 36 (12) (2015) 1425–1432.
[8] S. Perazzolo, R.M. Lewis, B.G. Sengers, Modelling the effect of intervillous flow on solute transfer based on 3D imaging of the human placental microstructure, Placenta 60 (2017) 21–27.
[9] R.M. Lewis, H. Baskaran, J. Green, S. Tashev, E. Palaiologou, E.M. Lofthouse, J. K. Cleal, A. Page, D.S. Chatelet, P. Goggin, B.G. Sengers, 3D visualization of trans-syncytial nanopores provides a pathway for paracellular diffusion across the human placental syncytiotrophoblast, iScience 25 (12) (2022) 105453.
[10] R.M. Lewis, Volume electron microscopy reveals placental ultrastructure in 3D, Placenta 141 (2023) 78–83.
[11] D. Laundon, O.L. Katsamenis, J. Thompson, P. Goggin, D.S. Chatelet, P. Chavatte-Palmer, N.J. Gostling, R.M. Lewis, Correlative multiscale microCT-SBF-SEM imaging of resin-embedded tissue, Methods Cell Biol. (2023) 241–267. Academic Press.
[12] K. Anderson, T. Nilsson, J. Fernandez-Rodriguez, Challenges for CLEM from a light microscopy perspective, in: P. Verkade, L.M. Collinson (Eds.), Correlative Imaging: Focusing on the Future, John Wiley & Sons Ltd, 2019, pp. 23–35.
[13] C.L. Fonta, B.M. Humbel, Correlative microscopy, Arch. Biochem. Biophys. 581 (2015) 98–110.
[14] O.L. Katsamenis, M. Olding, J.A. Warner, D.S. Chatelett, M.G. Jones, G. Sgalla, B. Smit, O.J. Larkin, I. Haig, L. Richeldi, I. Sinclair, P.M. Lackie, P. Schneider, X-Ray micro-computed tomography for nondestructive three-dimensional (3D) X-ray histology, Am. J. Pathol. 189 (8) (2019) 1608–1620.
[15] G. Wells, J.N. Glasgow, K. Nargan, K. Lumamba, R. Madansein, K. Maharaj, L. Y. Perumal, M. Matthew, R.L. Hunter, H. Pacl, J.E.P. Lever, D.D. Stanford, S. P. Singh, P. Bajpai, U. Manne, P.V. Benson, S.M. Rowe, S. le Roux, A. Sigal, M. Tshibalanganda, C. Wells, A. du Plessis, M. Msimang, T. Naidoo, A.J.C. Steyn, A high-resolution 3D atlas of the spectrum of tuberculous and COVID-19 lung lesions, EMBO Mol. Med. 14 (11) (2022).
[16] J. Frohn, D. Pinkert-Leetsch, J. Missbach-Guntner, M. Reichardt, M. Osterhoff, F. Alves, T. Salditt, 3D virtual histology of human pancreatic tissue by multiscale phase-contrast X-ray tomography, J. Synchrotron Radiat. 27 (2020) 1707–1719.
[17] S. Handschuh, C.T.C. Okada, I. Walter, C. Aurich, M. Glosmann, An optimized workflow for microCT imaging of formalin-fixed and paraffin-embedded (FFPE) early equine embryos, Anat. Histol. Embryol. 51 (5) (2022) 611–623.
[18] J. Schindelin, I. Arganda-Carreras, E. Frise, V. Kaynig, M. Longair, T. Pietzsch, S. Preibisch, C. Rueden, S. Saalfeld, B. Schmid, J.-Y. Tinevez, D.J. White, V. Hartenstein, K. Eliceiri, P. Tomancak, A. Cardona, Fiji: an open-source platform for biological-image analysis, Nat. Methods 9 (7) (2012) 676.
[19] O.L. Katsamenis, P.J. Basford, S.K. Robinson, XRH-processing-toolbox, zenodo.org (2023).
[20] O.L. Katsamenis, P.J. Basford, S.K. Robinson, R.P. Boardman, E. Konstantinopoulou, P.M. Lackie, A. Page, J.A. Ratnayaka, P. Goggin, G. J. Thomas, S.J. Cox, I. Sinclair, P. Schneider, A high-throughput 3D X-ray histology facility for biomedical research and preclinical applications, Wellcome Open Res 8 (2023).
[21] I. Belevich, M. Joensuu, D. Kumar, H. Vihinen, E. Jokitalo, Microscopy image browser: a platform for segmentation and analysis of multidimensional datasets, PLoS Biol. 14 (1) (2016).
[22] T.A.A. Tosta, P.R. de Faria, J.P.S. Servato, L.A. Neves, G.F. Roberto, A.S. Martins, M.Z. do Nascimento, Unsupervised method for normalization of hematoxylin-eosin stain in histological images, Comput. Med. Imag. Graph. 77 (2019).
[23] J.D. Bancroft, C. Layton, The hematoxylins and eosin, in: K.S. Suvarna, C. Layton, J.D. Bancroft (Eds.), Bancroft's Theory and Practice of Histological Techniques, Churchill Livingstone, 2012, pp. 173–186.
[24] S. Furukawa, Y. Kuroda, A. Sugiyama, A comparison of the histological structure of the placenta in experimental animals, J. Toxicol. Pathol. 27 (1) (2014) 11–18.
[25] J.A. Green, R.D. Geisert, G.A. Johnson, T.E. Spencer, Implantation and placentation in ruminants, Adv Anat Embryol Cel 234 (2021) 129–154.
[26] D.F. Antczak, W.R. Allen, Placentation in equids, Adv Anat Embryol Cel 234 (2021) 91–128.
[27] P. Chavatte-Palmer, E. Derisoud, M. Robles, Pregnancy and placental development in horses: an update, Domest. Anim. Endocrinol. 79 (2022).
[28] M.P. Kowalewski, A. Kazemian, K. Klisch, T. Gysin, M.T. Pereira, A. Gram, Canine endotheliochorial placenta: morpho-functional aspects, Adv Anat Embryol Cel 234 (2021) 155–179.

[29] D. Laundon, B.G. Sengers, J. Thompson, S.E. Harris, O. Beasley, P.J. Basford, O. L. Katsamenis, P. Goggin, E. Derisoud, D. Fanelli, C. Bocci, F. Camillo, J. Shotton, G. Constable-Dakeyne, N.J. Gostling, P. Chavatte-Palmer, R.M. Lewis, Convergently evolved placental villi show multiscale structural adaptations to differential placental invasiveness, Biol. Lett. 20 (3) (2024).

[30] I. Belevich, E. Jokitalo, DeepMIB: user-friendly and open-source software for training of deep learning network for biological image segmentation, PLoS Comput. Biol. 17 (3) (2021).

[31] I. Arganda-Carreras, V. Kaynig, C. Rueden, K.W. Eliceiri, J. Schindelin, A. Cardona, H.S. Seung, Trainable Weka Segmentation: a machine learning tool for microscopy pixel classification, Bioinformatics 33 (15) (2017) 2424–2426.

[32] S. Berg, D. Kutra, T. Kroeger, C.N. Straehle, B.X. Kausler, C. Haubold, M. Schiegg, J. Ales, T. Beier, M. Rudy, K. Eren, J.I. Cervantes, B.T. Xu, F. Beuttenmueller, A. Wolny, C. Zhang, U. Koethe, F.A. Hamprecht, A. Kreshuk, ilastik: interactive machine learning for (bio) image analysis, Nat. Methods 16 (12) (2019) 1226–1232.